Modeling Kinetic Shifts for Tight Transition States in Threshold Collision-Induced Dissociation. Case Study: Phenol Cation†

Felician Muntean‡ and P. B. Armentrout*

Department of Chemistry, University of Utah, Salt Lake City, Utah 84112

Received: February 19, 2002; In Final Form: April 2, 2002

A threshold collision-induced dissociation (CID) study is performed on the phenol cation dissociation, investigating the CO-loss channel. Quantum chemical calculations are performed on the system to investigate the details of the potential energy surface and to provide the molecular parameters necessary for CID cross-section modeling. The effects of kinetic shifts on the CID threshold determinations are investigated using a model that incorporates statistical unimolecular decay theory. The model is tested using unimolecular dissociation rate constants as a function of energy provided by earlier photoelectron−photoion coincidence (PEPICO) experiments. Calculations indicate that the rate-determining step is an initial enol−keto isomerization. When the calculated transition state that corresponds to this step is used in the unimolecular decay model, the PEPICO rates are reproduced very well. The dissociation thresholds derived from CID data are in reasonable agreement with the ones derived from fitting the PEPICO rates when similar transition-state assumptions are used. Final analysis of the CID data yields a 0 K dissociation energy for CO loss from phenol of 3.03 ± 0.14 eV, in good agreement with previously measured values. This indicates that the CID model correctly takes into account kinetic shifts for a tight transition state when positively identified by quantum chemical calculations.

Introduction

Threshold collision-induced dissociation (CID) has proven to be a robust means of determining the thermochemistry for a broad range of chemical systems.[1−9] The present paper is part of a series of studies designed to improve the accuracy of threshold CID by testing the validity of the procedures used in modeling, especially with regard to the treatment of kinetic shifts.[10−14] As described in a previous paper from this series,[15] the concept is to perform CID on a system for which both the energetics and the unimolecular dissociation rates as a function of energy are experimentally known. For such a system, uncertainties related to the ambiguity of transition state (TS) location and to the Rice−Ramsperger−Kassel−Marcus (RRKM) calculation[16] of unimolecular dissociation rates are largely eliminated. The system should also dissociate slowly enough to yield observable kinetic shifts on our instrument (slower than $(1-5) \times 10^{-4}$ s). By using the experimental dissociation rates in our analysis and by comparing CID thresholds with the known energetics, we can obtain feedback to improve our model.

A previous study in this series[15] concerned the CID of the ortho and para dichlorobenzene molecular cations leading to atomic Cl loss. This system was selected as a model for a simple covalent bond-breaking dissociation of a moderately large molecule. The study indicated that selecting the correct transition state is crucial to obtaining reliable thermochemistry from CID data of large molecular systems. A loose transition state was expected for a simple bond-breaking dissociation, but the study revealed that a phase-space limit or orbiting transition state does not properly characterize the breaking of a covalent chemical bond. The study also emphasized the utility of detailed quantum chemical calculations for a correct characterization of the dissociation paths.

In the present paper, we investigate the dissociation of the phenol cation (reaction 1). This molecular system lies at the other extreme in that it involves a dissociation that involves a complex, multistep molecular rearrangement, characterized by tight and constrained transition states, and a large kinetic shift.

$$C_6H_5OH^+ \rightarrow C_5H_6^+ + CO \qquad (1)$$

The lowest-energy dissociation channel of the phenol cation is the elimination of CO, a reaction that has fascinated many chemists. The process has been studied using several techniques including electron impact ionization,[17] high-energy collision-induced dissociation,[18−21] ion kinetic energy spectrometry,[22] photoelectron−photoion coincidence spectroscopy (PEPICO),[23] time-resolved electron impact ionization,[24] time-resolved photoionization mass spectrometry (TPIMS),[25,26] and theoretical calculations.[27,28] The CO elimination proceeds with a large kinetic energy release, and it involves a significant reverse activation energy (i.e., the signs of a complex mechanism that received several interpretations). The results of kinetic energy release measurements of daughters of several $C_6H_6O^+$ isomers suggested to many researchers the possibility that an enol−keto isomerization[18,20,22] to the cyclohexadienone cation was involved in the dissociation. Other scenarios have alternatively proposed a linear, supposedly low-energy intermediate.[18,21] The $C_5H_6^+$ product was demonstrated[23] to have a cyclic (cyclopentadienyl) structure. An early theoretical study[27] using MINDO/3 semiempirical calculations resulted in the first coherent picture of the dissociation path, which involves several intermediates. The first step according to this study was the enol−keto isomerization to the cyclohexadienone cation, which was indicated to be the rate-limiting step. Very recently (during the

† Part of the special issue "John C. Tully Festschrift". Dedicated to John Tully on the occasion of his 60th birthday and recognizing his many contributions to theoretical studies of chemical dynamics.

* Corresponding author. E-mail: armentrout@chem.utah.edu.

‡ Current address: JILA, University of Colorado, Boulder, Colorado 80302.

10.1021/jp020464e CCC: $22.00
Published on Web 07/10/2002

TABLE 1: Thermochemistry Related to the Phenol Cation Dissociation by Loss of CO[a]

M	IE (M, eV)	$\Delta_f H^o$ (M, kJ/mol)	$\Delta_f H^o$ (M^+, kJ/mol)
C_6H_5OH	8.47(0.02)	−96.3(0.8)	721(2)
		−85.2	*732(2)*
C_5H_6	8.56(0.01)	131(4)	957(4)
			971(4)[b]
CO	14.0139(0.0003)	−110.53(0.17)	1241.6(0.2)
		−113.80(0.2)	*1238.3(0.2)*

[a] From ref 29 unless otherwise noted. Uncertainties in parentheses. Numbers in roman indicate 298 K values using the ion convention. Numbers in italics indicate 0 K values. [b] Converted to 0 K using the calculated frequencies from Table 3.

preparation of this paper), a more accurate quantum chemical calculation study[28] explored the potential energy surface of the CO loss from the phenol cation in greater detail. About 20 structures were investigated in this recent study, along with the corresponding transition states, to predict the most probable dissociation path. Among various pathways that lead to CO loss, the one with the lowest-energy rate-determining transition state again involved enol−keto isomerization as the first step, and this step was confirmed to be rate-determining. Alternative paths that involved CO loss from an open-ring intermediate were found to be significantly more energetic.

The thermochemistry of this dissociation is fairly well established for both the reactants and the products, a rare case among systems whose thermodynamic measurements are routinely affected by kinetic shifts. Relevant literature values[29] are presented in Table 1 and indicate that reaction 1 is endothermic by 125.2 ± 4.5 kJ/mol (1.30 ± 0.05 eV). The dissociation threshold for reaction 1 has also been measured by a variety of techniques. Among these, PEPICO,[23] time-resolved electron impact,[24] and TPIMS[26] provide the most reliable values (i.e., those that account for kinetic shifts). The 0 K thresholds obtained in these studies are 3.16 ± 0.10, 3.12 ± 0.10, and 2.93 ± 0.04 eV, respectively, which are considerably above the endothermicity of reaction 1. The accuracy of these values depends on a correct estimation of the molecular parameters in the RRKM calculation of the dissociation kinetics, a problem discussed in detail below. The photon energy dependence of the experimental dissociation rates has also been measured for reaction 1 by PEPICO[23] experiments. These provide us with a series of rates over an energy range that nicely overlaps that of threshold CID measurements.

The present work describes a threshold CID study of the phenol cation dissociation, reaction 1. Quantum chemical calculations are also performed on the system to obtain molecular parameters necessary for RRKM calculations. Dissociation thresholds are determined from the energy dependence of the CID cross sections by analysis using a model that incorporates RRKM theory to account for kinetic shifts.[12] The molecular parameters required by RRKM theory in this analysis are selected such that the calculated dissociation rates as a function of energy reproduce well the experimental rates provided by the previous PEPICO data.[23] Different possible sets of parameters for modeling of the CID experiment, their effect on the dissociation rates, and their effect on the final CID threshold determination are discussed.

Experimental Section

Instrumentation. The guided ion-beam tandem mass spectrometer used in this study has been previously described in detail.[30] Briefly, the instrument comprises an ion source, a mass selector, a reaction region surrounding an octopole ion guide, a second mass selector, and a detector. The ion source used here is a microwave discharge, followed by a flow tube, with He as a buffer gas at pressures ranging from 0.5 to 0.8 Torr. Vapors of phenol are introduced into the flow-tube ion source through the inlet port located about 0.5 m from the microwave discharge. Phenol cations are formed by collisions with He ions and metastables and are thermalized by many collisions (>10^4) with He in the flow. Sample ions drift out of the flow tube and are focused through two regions of differential pumping. They are then accelerated, focused into a magnetic field for mass selection, decelerated using an exponential retarder, and focused into the octopole ion-guide region. The present experiments were performed on a single-octopole ion-guide configuration of our instrument.[30]

The reaction cell is placed around the octopole, and CID with Xe takes place here. The energy spread of the reactant ion beam in this region is about 0.25 eV fwhm, as measured by retarding potential analysis, which also establishes the absolute zero of the reactant-ion kinetic energy within about 0.05 eV. Typical Xe pressures in the cell vary between 0.05 and 0.2 mTorr. Product and unreacted primary ions drift out of the octopoles, are focused into the second mass selector, a quadrupole mass filter, and are then detected by a Daly-type detector.[31] The method of measuring absolute integral cross sections on this instrument has been previously described in detail.[30] Briefly, intensities for reactant and all product ions are measured as a function of the interaction energy and target gas pressure in the collision cell and are then converted to cross sections. Energies are converted from the laboratory scale to the center-of-mass frame using $E_{CM} = E_{lab}M/(M + m)$, where M is the mass of the neutral reactant and m is the mass of the reactant ion.

Data Analysis. Thermodynamic information provided by the low-energy CID experiment is extracted from the energy dependence of the integral cross sections in the threshold region by fitting the data with an empirical model. The model[10,12,13,32−34] used with best results is represented by expression 2,

$$\sigma(E) = (n\sigma_0/E)\sum_i g_i \int_{E_0-E_i}^{E} [1 - e^{-k(\epsilon+E_i)\tau}](E - \epsilon)^{n-1}\, d\epsilon \quad (2)$$

where σ is the cross section, E is the relative collision energy, E_0 is the reaction threshold at 0 K, σ_0 is an energy-independent scaling factor, and n is an adjustable parameter that describes the energy deposition during collision.[14,34] The summation is over the ro-vibrational states of the reactant ion having energies E_i with populations g_i such that $\Sigma g_i = 1$. The integration is over the energy deposited into the ion by the collision, ϵ, and the exponential factor represents the probability of dissociation within the time window of the experiment. Here, τ is the average experimental time available for dissociation, and $k(\epsilon + E_i)$ is the unimolecular dissociation rate constant calculated using RRKM theory.[16] The expression in eq 2 is further convoluted over the kinetic energy distributions of the two reactants before comparison with the data.[30] If kinetic shifts are negligible, eq 2 collapses to the more familiar modified line-of-centers function.[32,34−36]

As previously discussed,[15] we used an energy-dependent treatment of the experimental time window available for dissociation in our instrument. The short limit of the time window is provided by ions that preserve their initial kinetic energy after collision (grazing collisions with no energy deposited). The long limit is provided by ions that move with the center-of-mass velocity after collision (all of the available kinetic energy is deposited into internal degrees of freedom).

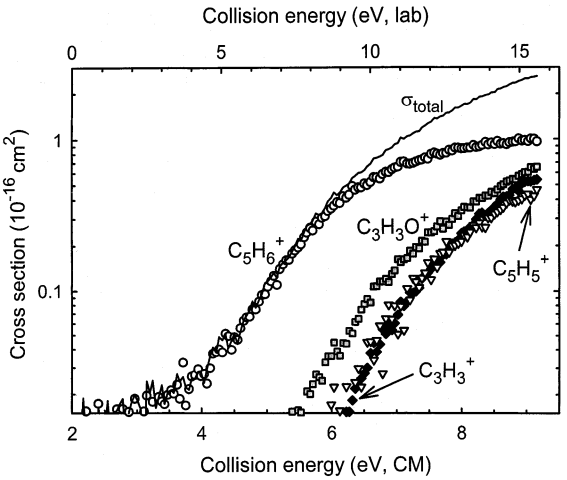

Figure 1. Integral cross sections as a function of energy for the CID of the phenol cation with Xe at a pressure of 0.1 mTorr.

Results

Integral Cross Sections. CID of the phenol cation with Xe as a neutral target is studied over the energy range from 0 to about 9 eV in the center-of-mass (CM) frame. The integral cross sections of the product ions observed in this energy range are presented in Figure 1. The dominant product ion observed and the first to appear as a function of energy is $C_5H_6^+$ at 66 amu, a result of process 1. The other products observed are $C_3H_3O^+$ (55 amu), $C_3H_3^+$ (39 amu), and $C_5H_5^+$ (65 amu). These higher-energy processes probably correspond to alternative dissociation paths, reactions 3 and 4, and a subsequent dissociation of the $C_5H_6^+$ primary ion, process 5, respectively. It is possible that $C_3H_3^+$ might be a decomposition product of $C_5H_6^+$; however, the energetics of the observed process relative to the minor products observed is more consistent with reaction 4. Under our experimental conditions, the $C_5H_5^+$ peak was incompletely resolved from the much more intense $C_5H_6^+$ peak, so the cross section shown in Figure 1 has been corrected for mass overlap. These minor channels will not be discussed further.

$$C_6H_5OH^+ \rightarrow C_3H_3O^+ + C_3H_3 \quad (3)$$

$$\rightarrow C_3H_3^+ + C_3H_3O \quad (4)$$

$$C_5H_6^+ \rightarrow C_5H_5^+ + H \quad (5)$$

The CID cross sections show a small tail (about 1−2% of the maximum cross section) at low energies, which is especially visible in the $C_5H_6^+$ cross section in Figure 1. The tail increases slightly with the He pressure in the flow-tube ion source whereas the main part of the $C_5H_6^+$ cross section decreases. This behavior generates a variation of the absolute cross section magnitudes for data sets taken at slightly different He pressures. The pressure dependence of the tail indicates that it results from internally excited ions formed by collisions in the differential pumping region immediately after the flow tube. Because of the low magnitude of the tail, the energy dependence of the $C_5H_6^+$ cross section is negligibly affected for most of the energy range investigated, except at the lowest energies. As a consequence, the tails do not influence the results of our threshold analyses of the CID cross sections, but because they do limit the sensitivity of our modeling by introducing a background signal, the tails were subtracted from the data files prior to modeling. In addition, we observe a weak dependence of the cross section on the pressure of the Xe gas used in the collision cell. Therefore, the CID cross sections are extrapolated to zero pressure of Xe[35,37] prior to modeling.

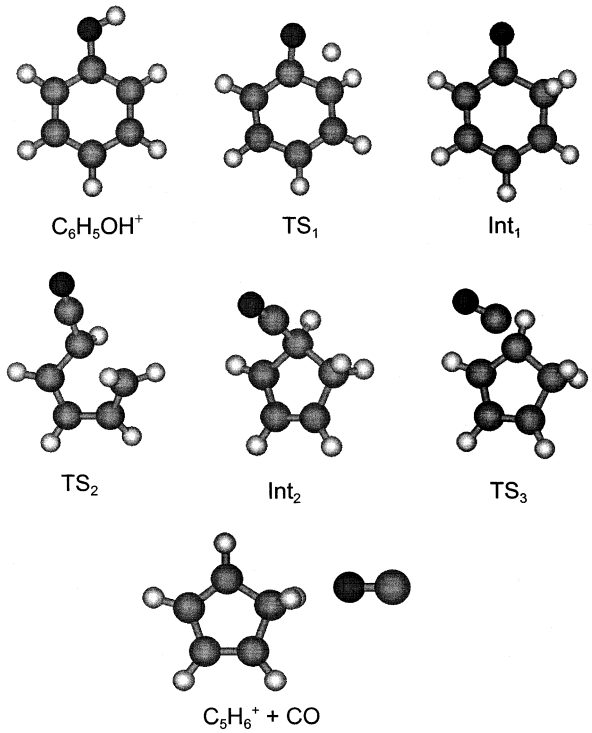

Figure 2. Optimized structures related to the phenol cation dissociation by loss of CO calculated at the B3LYP/6-31G* level of theory. The transition states (TSs) were found by reaction-path calculations between the two adjacent structures followed by quadratic synchronous transit calculations, all performed at the same level of theory.

Theoretical Results. Quantum chemical calculations on the phenol cation dissociation 1 are carried out using the Gaussian 98 program.[38] These results were obtained independently, and probably concomitantly, with another theoretical study published recently by Le et al. at a B3LYP/6-311++G(d,p) level for both geometry optimizations and single-point energies.[28] These authors calculated vibrational frequencies used in zero-point energy (ZPE) corrections at the B3LYP/6-31G(d,p) level and verified the single reference character of the wave functions by carrying out CASSCF(7,8)/6-31G(d,p) calculations on the B3LYP optimized geometries. Single-point energy calculations at the CASPT2(7,8)/6-31G(d,p) level (corrected for ZPE) were carried out for the reactant and all intermediates and transition states but could not be performed for the separated products.

In our study, geometry optimizations and vibrational frequency calculations on the reactant, products, transition states, and intermediates of process 1 were performed at the B3LYP/6-31G(d) level. Results of a previously reported MINDO/3 calculation[27] were used as starting points in optimizing some of the intermediate structures found. The transition states were obtained by detailed reaction-path calculations between each neighboring intermediate and were located using the quadratic synchronous transit approach of Schlegel and co-workers.[39,40] Frequency calculations verified the character of each stationary point. The optimized structures are presented in Figure 2 as a succession of stable intermediates (Int_1, Int_2) and connecting transition states (TS_1, TS_2, TS_3) along the CO-loss dissociation path. Single-point energy calculations are performed on the same systems at both the B3LYP/6-311++G(2d,2p)//B3LYP/6-31G(d) and MP2(full)/6-311++G(2d,2p)//B3LYP/6-31G(d) levels and for the reactant, products, and TS_1 also at the MP2(full)/6-311++G(2d,2p)//MP2(full)/6-31G(d) level. The results are

TABLE 2: Calculated Energies for Structures Related to the Phenol Cation Dissociation[a]

species	energy (hartrees)	ZPE (hartrees)[b]	relative energy (eV)	relative energy (eV)[c]
$C_6H_5OH^+$	−306.549225	0.102783	0	0
	−307.265193			
	−306.552393			
TS_1	−306.419108	0.095257	3.336	3.01
	−307.152090		*2.873*	*2.86*
	−306.424043		**3.288**	
Int_1	−306.484613	0.100268	1.690	1.49
	-307.218145		*1.212*	*1.51*
TS_2	−306.465187	0.097824	2.152	2.43
	−307.17765		*2.247*	*2.23*
Int_2	−306.511562	0.099491	0.935	1.05
	−307.207312		*1.485*	*1.42*
TS_3	−306.496967	0.098281	1.300	1.42
	−307.198805		*1.684*	*1.64*
$C_5H_6^+$	−193.368891	0.090894	0.889	1.20
	−193.860406		*1.256*	
	−193.369324		**0.973**	
CO	−113.140712	0.004933		
	−113.351681			
	−113.140347			

[a] Upper values indicate calculations at the MP2(full)/6-311++G(2d,2p)//B3LYP/6-31G(d) level, except for the zero-point energies (see below). Values in italics indicate calculations at the B3LYP/6-311++G(2d,2p)//B3LYP/6-31G(d) level, and values in bold indicate calculations at the MP2(full)/6-311++G(2d,2p)//MP2(full)/6-31G(d) level. [b] Zero-point energies (ZPE) are calculated at the B3LYP/6-31G(d) level and are scaled by a factor of 0.9804.[41] [c] CASPT2(7,8)/6-31G(d,p)//B3LYP/6-311++G(d,p) and (in italics) B3LYP/6-311++G(d,p)//B3LYP/6-311++G(d,p) values including zero-point energy corrections from Le et al.[28]

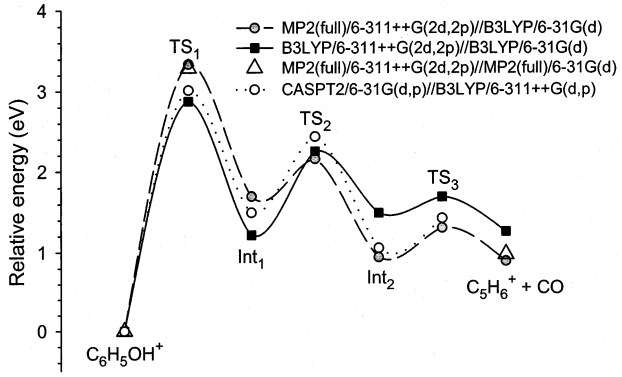

Figure 3. Schematic representation of the calculated energies for the structures (intermediates and transition states) related to the phenol cation dissociation by the loss of CO. The levels of calculation are shown. The energies are given relative to the energy of the phenol cation and include the zero-point energies calculated at the B3LYP/6-31G(d) level and scaled by 0.9804. CASPT2//B3LYP values are from Le et al.[28]

presented in Table 2 and Figure 3. We will refer to these various calculations as the B3LYP//B3LYP, MP2//B3LYP, and MP2//MP2 methods, respectively.

The first intermediate found, Int_1 (see Figure 2), is the 2,4-cyclohexadienone cation, formed by a 1,3 hydrogen shift from the phenol cation structure. This isomer is less stable than the phenol cation by about 1.2−1.7 eV (Table 2 and Figure 3). The transition state, TS_1, connecting the phenol cation to Int_1 is closer to the latter in geometry and is situated at a considerably high energy with respect to that of the phenol cation, 2.9−3.3 eV (Table 2). The second intermediate, Int_2, has a cyclopentadienyl−CO ($C_5H_6^+$−CO) structure (Figure 2). It proceeds from Int_1 by breaking the methylene−carbonyl bond, followed by forming a bond between the methylene and the carbon atom adjacent to the carbonyl. The stability of Int_2 relative to that of Int_1 is highly dependent on the methods used for calculation: 0.8 eV more stable for MP2//B3LYP and 0.3 eV less stable for B3LYP//B3LYP. The calculations of Le et al. indicate that Int_2 is more stable by 0.1 and 0.4 eV at the B3LYP//B3LYP and CASPT2//B3LYP levels, respectively.[28] The transition state, TS_2, that connects Int_1 and Int_2 is closer in geometry to the structure of the latter and is situated 0.5 and 1.0 eV above the energy of Int_1 for MP2//B3LYP and B3LYP//B3LYP calculations, respectively. Finally, the transition state, TS_3, that connects the second intermediate to the products is situated 0.2−0.4 eV above the energy of Int_2 and about 0.4 eV above the energy of the products (Table 2 and Figure 3).

We can compare our calculated energies with the known reaction endothermicity, 1.30 ± 0.05 eV (Table 1). This value is in very good agreement with the value from the B3LYP//B3LYP calculation, 1.26 eV, whereas the agreement with any of the MP2 calculations, 0.89 and 0.97 eV, is less satisfactory. The B3LYP calculation of Le et al., which uses a larger basis for the geometry optimization but a slightly smaller basis for the single-point energies, is in slightly worse agreement at 1.20 eV.[28]

All of the structures calculated here as part of the CO-loss dissociation path are very similar to the ones reported by Le et al.[28] in their detailed investigation of this potential energy surface. These authors investigated several alternate dissociation pathways, but the one with the rate-determining transition state having the lowest energy corresponds to the pathway described here. Along this reaction path, Le et al. find two additional intermediates: one is an open-ring structure between our Int_1 and Int_2, and the other is a weakly bound, product-like structure, the last step before products. As in our work, the transition state, TS_1, was found to be the rate-determining one. Our calculated energies are in very good agreement with the ones reported by Le et al. for all the commonly investigated structures (Table 2), which is not surprising given the rather similar levels of calculation, B3LYP/6-311++G(d,p)//B3LYP/6-311++G(d,p) in Le et al.[28] versus B3LYP/6-311++G(2d,2p)//B3LYP/6-31G(d) in this work. The only exception is the energy calculated for the structure that is equivalent to our Int_1, which is about 0.3 eV less stable in the B3LYP calculation of Le et al.[28] than in our B3LYP//B3LYP calculation. Their CASPT2//B3LYP energies are also similar to those calculated here (Table 2 and Figure 3).

Dissociation Rate Modeling. The unimolecular dissociation rates as a function of the internal energy of the system obtained in the PEPICO experiments[23] for process 1 are reproduced here using RRKM theory. The rates are evaluated using the vibrational frequencies and rotational constants calculated at the B3LYP/6-31G(d) level, with vibrations scaled by 0.9804,[41] as given in Table 3. A reaction degeneracy of 1 is assumed for all of the calculations (a value determined from the rotational symmetry numbers of the energized molecule and transition state).[42] As appropriate for the PEPICO experimental conditions, the rotational modes of the TS are treated as having a thermal, room-temperature distribution. The initial internal energy of the reactants is taken into account by simply shifting the energy scale of the rate constants by the average internal energy of phenol cations at room temperature (∼0.12 eV), as calculated using the vibrational frequencies in Table 3. When we apply

TABLE 3: Vibrational Frequencies and Rotational Constants Used in Modeling CID and Rate Constant Data for the $C_6H_5OH^+$ Dissociation to $C_5H_6^+ + CO$

species	vibrational frequencies (cm^{-1})[a]	rotational constant (cm^{-1}) 1D	rotational constant (cm^{-1}) 2D
$C_6H_5OH^+$	184, 356, 407, 430, 516, 558, 607, 612, 780, 791, 806, 927, 974, 980, 982, 998, 1087, 1133, 1178, 1190, 1350, 1379, 1391, 1432, 1491, 1525, 1636, 3147, 3164, 3172, 3177, 3182, 3577	0.179	0.074
$C_5H_6^+$	279, 429, 638, 800, 802, 813, 898, 943, 956, 992, 1016, 1096, 1112, 1136, 1160, 1317, 1353, 1400, 1465, 1471, 1494, 3038, 3060, 3247, 3252, 3260, 3269	0.142	0.276
CO	2209		1.899
TS_1[b]	181, 309, 412, 448, 526, 572, 619, 744, 768, 819, 866, 947, 966, 979, 1006, 1043, 1088, 1143, 1165, 1252, 1330, 1393, 1414, 1450, 1500, 1523, 1639, 3016, 3160, 3166, 3174, 3179	0.168	0.078
TS_{FM}[c]	196 (2), 244, 309, 403, 503, 516(2), 556, 686 (2), 751, 815, 817, 881, 972, 976, 995, 1024, 1040, 1210, 1395, 1472, 1500, 1603, 1669, 3027, 3049, 3063, 3070, 3087, 3656	0.190	0.085

[a] Calculated at the B3LYP/6-31G(d) level and scaled by a factor of 0.9804.[41] [b] Calculated transition state, TS_1. [c] Frequencies assumed by Fraser-Monteiro et al.[23] Degeneracies are given in parentheses.

the more complicated, correct procedure of convoluting the calculated rates over the internal energy distribution of the phenol cations at room temperature, we obtain similar results mainly because the energy range of the rate data is much higher than the dissociation thresholds, as originally pointed out in the PEPICO study.[23] Several possible assumptions about the TS are made, as discussed below. For each TS assumed, the value of the activation energy (the 0 K dissociation threshold) is varied until the best agreement with the data is obtained. The results are presented in Figure 4. The uncertainties in the dissociation energies derived from fitting the unimolecular dissociation rates are assigned to the same value as that reported in the original PEPICO experiments, 0.1 eV.

The first transition state considered is the calculated TS_1 (Tables 2 and 3 and Figures 2 and 3), which connects the reactant to Int_1, the cyclohexadienone cation intermediate. The fact that it is the first step in a series of geometrical changes leading to dissociation, along with the fact that it represents the highest energetic barrier, makes this transition state the most probable candidate for the rate-determining transition state. This is also supported by other theoretical investigations.[27,28] The best reproduction of the experimental PEPICO rates is achieved when the dissociation threshold is set to 2.87 eV. The calculated rates have a slope that is slightly lower than that of the PEPICO data, as observed in Figure 4, although within experimental error. This indicates that a better reproduction of the rate data would be achieved by a transition state that is slightly looser. To losen TS_1, we tried scaling the calculated vibrational frequencies by different amounts. When using a factor of 0.93, the rates calculated with "TS_1 scaled" give an excellent fit to the rate data, as observed in Figure 4, for a threshold value of 2.98 eV.

Rate constants evaluated using molecular parameters for the other calculated transition states (TS_2 and TS_3) have significantly higher slopes than the PEPICO data, an indication that they promote unrealistically fast dissociations. Similar results were obtained by Caballol et al.[27] in previous theoretical work. Their investigation confirmed that the rate constants calculated for a transition state similar to our TS_1 are orders of magnitude lower than those for any of the other two transition states at energies within the range of the PEPICO data. This indicates that the choice of TS_1 as the rate-determining transition state is a reasonable one.

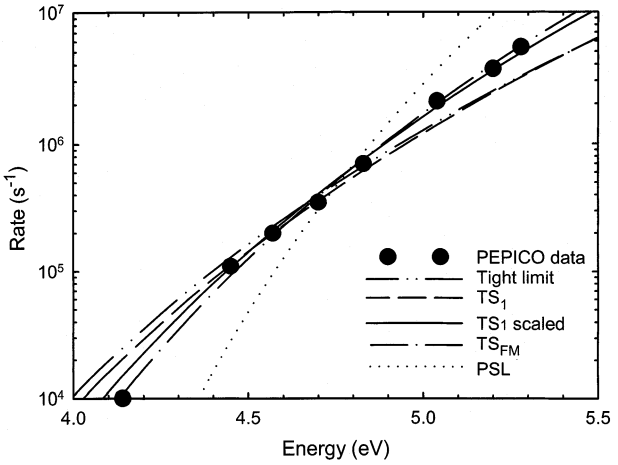

Figure 4. RRKM modeling of unimolecular dissociation rates as a function of energy obtained in the PEPICO experiment[23] for the phenol cation dissociation by the loss of CO (●). The energy scale represents the photon energy of the PEPICO experiment plus the average thermal energy of the phenol cations (~0.12 eV) minus the ionization energy of the phenol cations (8.47 eV). The lines represent RRKM rates calculated using different transition-state assumptions: the theoretical rate-determining transition state, TS_1 (− − −); the transition state TS_1 with vibrational frequencies scaled by 0.93 (—); the phase-space-limit (PSL) transition state (· · ·); the tight-limit transition state (− · · −); and the transition state used by Fraser-Monteiro et al.[23] (− · −). The particular thresholds used are described in the text and in Table 4.

Two other transition states are also investigated at the loose and tight limits, which correspond to the fastest and slowest possible dissociation, respectively. The loose limit is represented by a transition state at the phase-space limit (PSL) in which the incipient product fragments are allowed to rotate freely. In our analysis program, such a transition state is located at the centrifugal barrier appropriate for an ion−induced dipole potential.[12] The molecular parameters of such a transition state (PSL TS) are given simply by the vibrations and rotational

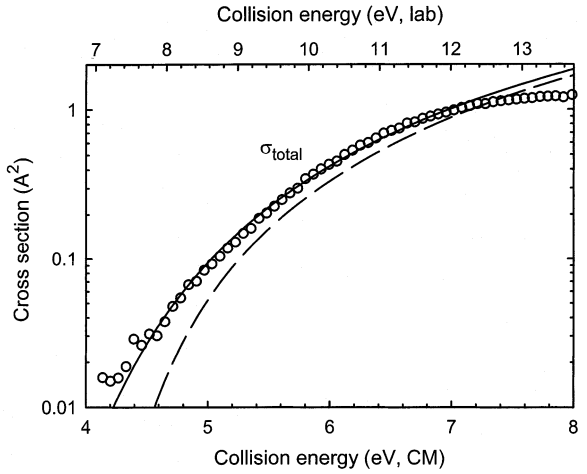

Figure 5. Modeling of the total cross section for CID of the phenol cation with Xe using eq 2 with parameters indicated in Table 4 and the TS_1 scaled transition state. The symbols represent the total cross section data extrapolated to zero Xe pressure, the dashed line represents the model for reactants with an internal temperature of 0 K, and the solid line represents the same model convoluted over the kinetic and internal energy distributions of the two reactants.

constants of the two products (Table 3), as previously described.[12] The threshold energy is adjusted in an attempt to reproduce the PEPICO rates, with the best agreement achieved for a value of 3.85 eV, although the slope of the calculated rates is substantially higher than that of the rate data, which is significantly outside experimental uncertainties (Figure 4). As expected, this indicates that a PSL loose TS is not an appropriate choice for this dissociation, but it provides a safe upper limit to the dissociation threshold when transition-state calculations are not available. The tight limit is represented by a transition state with molecular parameters identical to those of the parent phenol cation except that the frequency corresponding to the reaction coordinate is removed. Here, we assumed that a reasonable reaction coordinate frequency is a C−C stretch frequency of about 1200 cm^{-1}. The rates calculated with this simple assumption have a smaller slope in the region of comparison with the PEPICO data (Figure 4). The agreement is best when the threshold value is 2.85 eV. This value represents a reasonable lower limit to the dissociation threshold.

It is also worth discussing the RRKM calculation of Fraser-Monteiro et al.[23] in which experimental PEPICO rates were reproduced with a threshold value of 3.12 eV. In their calculation, because of the lack of available calculated frequencies, the authors assembled a set of reasonable frequencies for the phenol cation on the basis of a series of 14 measured frequencies. For the transition state (TS_{FM}, Table 3), they scaled down some of the phenol cation frequencies to different arbitrary extents until the best reproduction of experimental rates was achieved. We tried to reproduce their fits, and the results are shown in Figure 4. A very good fit is achieved when the threshold is set to 3.07 eV. This value is somewhat lower than the one reported by Fraser-Monteiro et al. (3.12 ± 0.10 eV), but the small difference probably results from slightly different details (e.g., the treatment of rotations) or algorithms of the RRKM rate calculations in the two studies.

CID Cross-Section Modeling. CID cross sections are modeled using the procedure described in the data analysis section. The model includes RRKM theory to account for kinetic shifts (eq 2) and is used with all of the transition states discussed above. A representative model fit to the CID data is presented in Figure 5 for TS_1 scaled, and the optimized thresholds obtained using the different TS assumptions are presented in Table 4. On the scale of Figure 5, the fits to the CID data obtained using the different TS assumptions look identical. The difference between them appears only at energies very close to those of the true thresholds and at cross sections that are much lower than the background noise in the data. Uncertainties in the threshold energies are calculated by considering a series of sources of error: the variation of optimized fit parameters among different data files, the range of parameters that allow reasonably good reproduction of data, the uncertainty in the experimentally available time for dissociation (which leads to an uncertainty of ± 0.03 eV), and the uncertainty in the collision-energy calibration (± 0.05 eV, laboratory frame). The final results are presented in Table 4.

TABLE 4: Dissociation Energies and Entropies of Activation at 1000 K (J/K mol) for $C_6H_5OH^+$ Dissociation to $C_5H_6^+ + CO$

method			energy (eV)	$\Delta S^{\ddagger}_{1000}$ (J/K mol)
Calculation[a]				
		MP2//B3LYP	3.34	
		B3LYP//B3LYP	2.87	
		MP2//MP2	3.29	
		CASPT2//B3LYP[b]	3.01	
Modeling				
	TS_1[c]	rate	2.87 ± 0.10	
		CID	2.97 ± 0.13	−4
	TS_1 scaled[d]	rate	2.98 ± 0.10	
		CID	3.03 ± 0.13	11
	PSL[e]	rate	3.85 ± 0.10	
		CID	3.72 ± 0.13	77
	tight limit[f]	rate	2.85 ± 0.10	
		CID	2.98 ± 0.13	−5
	TS_{FM}[g]	rate	3.07 ± 0.10	
		CID	3.09 ± 0.13	20
	no RRKM[h]	CID	4.07 ± 0.12	
	average[i]	rate	2.98 ± 0.10	
		CID	3.03 ± 0.14	
	literature	TEI (298 K)[j]	3.03 ± 0.10	9 ± 5
		PIMS[k]	2.93 ± 0.04	
		PEPICO[l]	3.12 ± 0.10	

[a] Calculated using the methods shown at the 6-311++G(2d,2p)//6-31G(d) level (Table 2). [b] Value from Le et al.[28] [c] Model using the calculated transition state, TS_1. [d] Model using TS_1 with vibrational frequencies scaled by 0.93. [e] Model using a phase-space limit loose transition state. [f] Model using a tight transition state. [g] Model using the vibrational frequencies and rotational constants assigned by Fraser-Monteiro et al.[23] [h] Modeling disregarding kinetic shifts. [i] Average from modeling data and assuming only the calculated transition state (TS_1 scaled) that accurately reproduces the PEPICO rates. The other parameters used in modeling CID data with the model of eq 2 are $\sigma_0 = 0.5 \pm 0.2$ and $n = 2.4 \pm 0.4$. [j] Value from Lifshitz and Gefen.[24] [k] Value from Malinovitch and Lifshitz.[26] [l] Value from Fraser-Monteiro et al.[23]

The fit obtained by using the calculated TS_1 gives a threshold of 2.97 ± 0.13 eV. This is a fairly tight transition state, as indicated by the small negative entropy of activation ($\Delta S^{\ddagger}$ = −4 J/K mol, which is listed in Table 4 at 1000 K). Indeed, this fit is essentially equivalent to that at the tight-limit transition state, which has a threshold of 2.98 ± 0.13 eV and a $\Delta S^{\ddagger}$value of −5 J/K mol. The tight limit assumes the slowest dissociation possible and results in the largest kinetic shifts. Thus, these analyses yield lower limits to the true CID threshold. The fit made by using the PSL transition state, PSL TS, gives a threshold of 3.72 ± 0.13 eV. This model is the loose limit to a

transition state and therefore assumes the fastest dissociation possible for the system. It results in the lowest experimental kinetic shift and the largest CID threshold that could be attributed to the system in the absence of other information like the PEPICO dissociation rate or calculations. The looseness of this TS is indicated by the very large positive entropy of activation ($\Delta S^{\ddagger} = 77$ J/K mol, Table 4). The threshold value obtained with PSL TS is not particularly meaningful, however, because no good fit to the PEPICO rates was possible using this transition state, as shown in Figure 4. When the TS_1 scaled model is considered, the CID fit gives a threshold of 3.03 ± 0.13 eV and a positive value for the entropy of activation, 11 J/K mol, that indicates a slightly looser transition state than the tight limit. This entropy of activation is in good agreement with that deduced by Malinovich and Lifshitz (9 ± 5 J/K mol, Table 4).[26] We also modeled CID cross sections by using TS_{FM}, the transition state with vibrational frequencies selected by Fraser-Monteiro et al.[23] Here, the entropy of activation is a slightly larger positive value, indicating a moderately loose transition state. A CID threshold of 3.09 ± 0.13 eV is obtained in this case.

The cross sections are also analyzed using the basic CID model that disregards the kinetic shift effects (Table 4). This model is the limit of eq 2 when the time window of the experiment τ approaches infinity. Differences between the threshold values determined above and the one determined using this basic model, 4.07 ± 0.12 eV, indicate that the kinetic shift for this system as determined on our instrument is about 1.0 eV.

Discussion

The complexity of accounting for kinetic shifts in CID is increased by the fact that the part of the cross section whose shape is most affected by kinetic shifts (the lowest energies) is usually obscured in the noise. As a result, the model of eq 2 reproduces the CID cross sections equally well for any of the TS assumptions discussed above, so we cannot judge the proper choice of a transition state on the basis of CID data reproduction alone. This fact has also been observed for other systems, as pointed out in a previous study.[15] However, because the present system was especially selected as a case study, we have other information that we can use in judging a correct transition state. In addition to theoretical calculations, we have unimolecular dissociation rate data and other literature values for the dissociation threshold to compare with.

Quantum chemical calculations applied to a molecular dissociation potential energy surface can be used to locate the rate-determining transition state. A particular exception is when the dissociation involves simple bond breaking (i.e., when the transition state cannot be associated with a stationary point along the potential energy surface, a case of which has been recently discussed[15]). For the present system, the rate-determining transition state is positively identified as TS_1, the enol−keto isomerization transition state, by a series of theoretical studies that included the semiempirical calculations of Caballol et al.[27] and the quantum chemical calculations of Le et al.[28] and the present work. The only uncertainty that remains concerning this transition state is related to the proper scaling of the calculated vibrational frequencies.

Unimolecular dissociation rate data as a function of energy are an excellent complement to theory in determining the correct choice of a transition state. PEPICO data[23] in this case provide a test of whether our choice of TS_1 for the rate-determining transition state is correct. In addition, the best scaling factor for the calculated frequencies is obtained by comparing our calculated RRKM dissociation rates using TS_1 with the experimental PEPICO rates. This comparison can also help us find a value for the uncertainty in the true threshold that is related to transition-state selection. In this case, we do this by varying the scaling of the transition-state frequencies and by finding the corresponding range of dissociation thresholds such that the calculated RRKM rates still reproduce the PEPICO data. Finally, we limit the acceptable CID thresholds to the ones obtained under the assumptions that also lead to good RRKM fits of the PEPICO dissociation rates. Combining all reasonable TS assumptions and all sources of uncertainty, we thus obtain a value of 3.03 ± 0.14 eV for the 0 K CID threshold for CO loss from the phenol cation.

We can now compare our CID threshold value with the other known values from the literature (Table 1). The agreement is good, within uncertainty, with both the 3.12 ± 0.10 eV value from the PEPICO study of Fraser-Monteiro et al.[23] and the 2.93 ± 0.04 value from the PIMS study of Malinovitch and Lifshitz.[26] Notice that these two values do not agree with one another within their uncertainties. Both of these values are derived using RRKM fits to experimental data and are therefore dependent on the choice of the proper transition state. In the work of Fraser-Monteiro et al.,[23] the transition-state parameters were somewhat arbitrary, chosen partially on the basis of the vibrational frequencies of the parent molecules and partially to provide the best RRKM fit to the PEPICO data. Further, as demonstrated above, the PEPICO data can be reproduced well using the calculated transition state TS_1 scaled (Figure 4), with a lower threshold value of 2.98 ± 0.10 eV. This latter value is now more consistent with the determination of Malinovitch and Lifshitz,[26] who performed a rather detailed sensitivity analysis on the TS assumptions in their study. Finally, the time-resolved electron ionization value of Lifshitz and Gefen[24] is 3.03 ± 0.10 eV for a 298 K dissociation threshold. If we convert to 0 K, we obtain an approximate value of 3.16 ± 0.10 eV, which is in agreement with our CID value within the combined uncertainties.

It is also interesting to compare the dissociation thresholds obtained using the three methods involved in this study: analysis of the unimolecular dissociation rates, analysis of CID cross sections, and calculations. As observed in Table 4, the thresholds derived by fitting the PEPICO unimolecular dissociation rates are in reasonable agreement with the ones derived from CID when similar TS assumptions are involved. The former are generally somewhat lower than the latter (except for the PSL TS where the threshold values are less meaningful) but within the uncertainties. It is interesting to note that the agreement is very good (within 0.05 eV) in cases when the fit to the experimental rates (Figure 4) is good, TS_1 scaled and TS_{FM}. The calculated thresholds (energy of TS_1 relative to that of the phenol cation) vary significantly with the method used, as shown in Table 4. The best agreement with either the CID or the rate values is obtained for the CASPT2//B3LYP calculations of Le et al.[28] Our B3LYP//B3LYP value is in reasonable agreement, being within 0.16 eV of the CID average and within 0.11 eV of the rate average. It is worth noting that this B3LYP//B3LYP combination yielded the best agreement with the literature value of the reaction endothermicity, within 0.04 eV, as discussed in the Results section above. The agreement of the dissociation thresholds with any of the MP2 calculations is less satisfactory, differing by about 0.3 eV from the CID value (Table 4).

Finally, we can estimate what our CID results would be if we did not have a set of PEPICO rate data available, as will

generally be the case. With the rate-determining transition state identified by calculations as TS_1 and without the feedback on vibrational frequency scaling from the PEPICO rates, we would set the threshold value at 2.97 ± 0.14 eV, where the error includes contributions from using vibrational frequencies scaled by 5%. This value is 0.06 eV lower than our best value of 3.03 ± 0.14 eV but is still well within our experimental uncertainties.

Conclusions

Collision-induced dissociation of the phenol cation is investigated over an energy range from 0 to 9 eV in the center-of-mass frame. The present study investigates in detail the dissociation channel involving the loss of CO. Quantum chemical calculations complement the experiments and provide details of the dissociation mechanism, equilibrium geometries, energies, and vibrational frequencies for reactants, products, and intermediates of this dissociation. The dissociation is found to proceed through an enol−keto isomerization step, which is the rate-determining step, in agreement with other calculations.[27,28] The calculated reaction endothermicity of 1.26 eV at the B3LYP/6-311++G(2d,2p)//B3LYP/6-31G(d) level is in good agreement with the literature value of 1.30 ± 0.05 eV.

Different assumptions about the transition state are tested by comparing RRKM calculations with unimolecular dissociation rate constants as a function of energy, as determined in previous PEPICO experiments.[23] The transition state calculated for the rate-determining dissociation step, TS_1, provides the best fit to the PEPICO rates when its vibrational frequencies are scaled by a factor of 0.93. The RRKM analysis of the PEPICO rates using the calculated transition state after vibrational frequency scaling, TS_1 scaled, yields a dissociation threshold of 2.98 ± 0.10 eV, which is 0.14 eV lower than the value determined by Fraser-Monteiro et al. on the basis of a somewhat more arbitrary transition state defined in the absence of quantum chemical calculations.

The CID cross sections are modeled using a range of transition states that successfully reproduce the PEPICO rates. The resulting average CID threshold for the loss of CO at 0 K is 3.03 ± 0.14 eV. The CID threshold is in reasonable agreement, within uncertainties, with the other experimental values: 3.12 ± 0.10 eV from PEPICO,[23] 2.98 ± 0.10 eV from our reanalysis of the PEPICO data, 3.16 ± 0.10 eV from time-resolved electron impact measurements,[24] and 2.93 ± 0.04 eV from PIMS.[26] These values agree very well with the value of 3.01 eV that was calculated by Le et al. at the CASPT2(7,8)/6-31G(d,p)//B3LYP/6-311++G(d,p) level. In the calculations performed here, the dissociation energy determined at the B3LYP/6-311++G(2d,2p)//B3LYP/6-31G(d) level yields 2.87 eV, which is in better agreement with the CID value than when MP2 methods are used.

The study indicates that the CID model correctly takes into account kinetic shifts on the order of 1 eV in dissociations involving tight transition states, which can be identified by quantum chemical calculations.

Acknowledgment. This work is supported by the National Science Foundation, Grants No. CHE 9877162 and 0135517.

References and Notes

(1) Tiernan, T. O.; Wu, R. L. *Adv. Mass Spectrom.* **1978**, *7A*, 136.

(2) Squires, R. R. *Int. J. Mass Spectrom. Ion Processes* **1992**, *117*, 565.

(3) Magnera, T. F.; David, D. E.; Michl, J. *J. Am. Chem. Soc.* **1989**, *111*, 4100.

(4) Armentrout, P. B. *Acc. Chem. Res.* **1995**, *28*, 430.

(5) Klassen, J. S.; Anderson, S. G.; Blades, A. T.; Kebarle, P. *J. Phys. Chem.* **1996**, *100*, 14218.

(6) Grushow, A.; Ervin, K. M. *J. Am. Chem. Soc.* **1995**, *117*, 11612.

(7) Sowa-Resat, M. B.; Hintz, P. A.; Anderson, S. L. *J. Phys. Chem.* **1995**, *99*, 10736.

(8) Deng, H. T.; Kerns, K. P.; Castleman, A. W. *J. Phys. Chem.* **1996**, *100*, 13386.

(9) Amunugama, R.; Rodgers, M. T. *Int. J. Mass Spectrom.* **2000**, *195/196*, 439.

(10) Loh, S. K.; Hales, D. A.; Lian, L.; Armentrout, P. B. *J. Chem. Phys.* **1989**, *90*, 5466.

(11) Khan, F. A.; Clemmer, D. E.; Schultz, R. H.; Armentrout, P. B. *J. Phys. Chem.* **1993**, *97*, 7978.

(12) Rodgers, M. T.; Ervin, K. M.; Armentrout, P. B. *J. Chem. Phys.* **1997**, *106*, 4499.

(13) Rodgers, M. T.; Armentrout, P. B. *J. Chem. Phys.* **1998**, *109*, 1787.

(14) Muntean, F.; Armentrout, P. B. *J. Chem. Phys.* **2001**, *115*, 1213.

(15) Muntean, F.; Heumann, L.; Armentrout, P. B. *J. Chem. Phys.* **2002**, *116*, 5593.

(16) See, for example, Gilbert, R. G.; Smith, S. C. *Theory of Unimolecular and Recombination Reactions*; Blackwell Scientific Publications: Oxford, 1990.

(17) Henion, J. D.; Kingston, D. G. I. *J. Am. Chem. Soc.* **1973**, *95*, 8358.

(18) Maquestiau, A.; van Haverbeke, Y.; Flammang, R.; Meyer, C. D.; Das, K. G.; Reddy, S. *Org. Mass Spectrom.* **1977**, *12*, 631.

(19) Russell, D. H.; Gross, M. L.; Nibbering, N. M. *J. Am. Chem. Soc.* **1978**, *100*, 6133.

(20) Russell, D. H.; Gross, M. L.; van der Greef, J.; Nibbering, N. M. *Org. Mass Spectrom.* **1979**, *14*, 474.

(21) Maquestiau, A.; Flammang, R.; Glish, G. L.; Laramee, J. A.; Cooks, R. G. *Org. Mass Spectrom.* **1980**, *15*, 131.

(22) Hoffman, M. K.; Friesen, M. D.; Richmond, G. *Org. Mass Spectrom.* **1977**, *12*, 150.

(23) Fraser-Monteiro, M. L.; Fraser-Monteiro, L.; de Wit, J.; Baer, T. *J. Phys. Chem.* **1984**, *88*, 3622.

(24) Lifshitz, C.; Gefen, S. *Org. Mass Spectrom.* **1984**, *19*, 197.

(25) Lifshitz, C.; Gefen, S.; Arakawa, R. *J. Phys. Chem.* **1984**, *88*, 4242.

(26) Malinovitch, Y.; Lifshitz, C. *J. Phys. Chem.* **1986**, *90*, 4311.

(27) Caballol, R.; Poblet, J. M.; Sarasa, J. P. *J. Phys. Chem.* **1985**, *89*, 5836.

(28) Le, H. T.; Flammang, R.; Gerbaux, P.; Bouchoux, G.; Nguyen M. T. *J. Phys. Chem. A* **2001**, *105*, 11582.

(29) Lias, S. G.; Bartmess, J. E.; Liebman, J. F.; Holmes, J. L.; Levin, R. D.; Mallard, W. G. *J. Phys. Chem. Ref. Data* **1988**, *17* (Supplement 1).

(30) Ervin, K. M.; Armentrout, P. B. *J. Chem. Phys.* **1985**, *83*, 166.

(31) Daly, N. R. *Rev. Sci. Instrum.* **1959**, *31*, 264.

(32) Levine, R. D.; Bernstein, R. B. *J. Chem. Phys.* **1972**, *56*, 281.

(33) Schultz, R. H.; Armentrout, P. B. *Int. J. Mass Spectrom. Ion Processes* **1991**, *107*, 29.

(34) Armentrout, P. B. *Int. J. Mass Spectrom.* **2000**, *200*, 219.

(35) Schultz, R. H.; Crellin, K. C.; Armentrout, P. B. *J. Am. Chem. Soc.* **1991**, *113*, 8590.

(36) Levine, R. D.; Bernstein, R. B. *Molecular Reaction Dynamics and Chemical Reactivity*; Oxford University Press: New York, 1987.

(37) Hales, D. A.; Lian, L.; Armentrout, P. B. *Int. J. Mass Spectrom. Ion Processes* **1990**, *102*, 269.

(38) Frisch, M. J.; Trucks, G. W.; Schlegel, H. B.; Scuseria, G. E.; Robb, M. A.; Cheeseman, J. R.; Zakrzewski, V. G.; Montgomery, J. A., Jr.; Stratmann, R. E.; Burant, J. C.; Dapprich, S.; Millam, J. M.; Daniels, A. D.; Kudin, K. N.; Strain, M. C.; Farkas, O.; Tomasi, J.; Barone, V.; Cossi, M.; Cammi, R.; Mennucci, B.; Pomelli, C.; Adamo, C.; Clifford, S.; Ochterski, J.; Petersson, G. A.; Ayala, P. Y.; Cui, Q.; Morokuma, K.; Malick, D. K.; Rabuck, A. D.; Raghavachari, K.; Foresman, J. B.; Cioslowski, J.; Ortiz, J. V.; Stefanov, B. B.; Liu, G.; Liashenko, A.; Piskorz, P.; Komaromi, I.; Gomperts, R.; Martin, R. L.; Fox, D. J.; Keith, T.; Al-Laham, M. A.; Peng, C. Y.; Nanayakkara, A.; Gonzalez, C.; Challacombe, M.; Gill, P. M. W.; Johnson, B. G.; Chen, W.; Wong, M. W.; Andres, J. L.; Head-Gordon, M.; Replogle, E. S.; Pople, J. A. *Gaussian 98*, revision A.3; Gaussian, Inc.: Pittsburgh, PA, 1998.

(39) Peng, C.; Ayala, P. Y.; Schlegel, H. B.; Frisch, M. J. *J. Comput. Chem.* **1996**, *17*, 49.

(40) Peng, C.; Schlegel, H. B. *Isr. J. Chem.* **1994**, *33*, 449.

(41) Foresman, J. B.; Frisch, A. E. *Exploring Chemistry with Electronic Structure Methods*, 2nd ed.; Gaussian, Inc.: Pittsburgh, PA, 1996.

(42) Gilbert, R. G.; Smith, S. C. *Theory of Unimolecular and Recombination Reactions*; Blackwell Scientific: Oxford, 1990.